Chemical Science

EDGE ARTICLE

View Article Online
View Journal | View Issue

Cite this: *Chem. Sci.*, 2018, **9**, 7483

All publication charges for this article have been paid for by the Royal Society of Chemistry

Treatment of hyperphosphatemia based on specific interactions between phosphorus and Zr(IV) active centers of nano-MOFs†

Wei Zhang,‡* Jiheng Xu,‡ Ping Li, Xiaonan Gao, Wen Zhang, Hui Wang and Bo Tang*

Hyperphosphatemia is closely associated with the occurrence of multiple organ dysfunctions in patients with end-stage renal disease (ESRD). The application of phosphorus binders as an effective clinical approach for such diseases still suffers from serious side effects. Therefore, development of new phosphorus binders for the treatment of hyperphosphatemia remains a great challenge. Herein, we describe a kind of zirconium (Zr(IV))-based nano-MOF that is well suited for specific adsorption and selective fluorescence sensing of phosphate, and is based on the particular interactions between Zr(IV) and phosphate. The reduced levels of phosphate were quantitatively monitored using the MOF-based fluorescence nanosensor. Notably, the MOFs exhibit a greater reduction in phosphorus levels than commercially available phosphorus binders, and comparable therapeutic effects in the treatment of hyperphosphatemia of a mice model. Hence, the MOF acts as a promising medication for hyperphosphatemia by directly adsorbing phosphorus in the blood, which offers new perspectives in future applications of MOFs.

Received 15th June 2018
Accepted 20th July 2018

DOI: 10.1039/c8sc02638f

rsc.li/chemical-science

Introduction

Chronic kidney disease, especially renal failure, has dramatically increased over the past few years as a serious global public problem which threatens humans.[1] Currently, hemodialysis as an effective renal failure therapy still experiences limitations in the removal of toxins that leads to the presence of metabolites in the body.[2–4] Moreover, hyperphosphatemia, considered to be a common metabolic complication in hemodialysis patients, was found to be key for raising serum phosphorus levels in chronic kidney disease-mineral and bone disorder (CKD-MB), thereby further increasing the occurrence and development of CKD-MB.[5,6] The main clinical manifestations of CKD-MB are hyperparathyroidism, abnormal mineral and bone metabolism, and calcification of blood vessels and other soft tissues. Such a disease not only increases the patients' morbidity and seriously influences their quality of life, but also increases the incidence of cardiovascular diseases and eventually death.[7–9] Hence, curing hyperphosphatemia has become quite crucial for the prevention and control of complications in hemodialysis patients, and urgently needs to be solved.

The phosphorus binders currently used for hyperphosphatemia treatment are aluminum, calcium and iron based binders, as well as $La_2(CO_3)_3$ *etc.*[10,11] However, these binders' side effects and their impact on the patient's prognosis remain a serious concern.[12,13] Take aluminum-based phosphorus binders for example: their toxicity for the central nervous system, blood system, and bones significantly limits their clinical applications. On the other hand, La accumulates in many organs such as the liver and kidneys, which causes adverse reactions like encephalopathy.[14,15] Therefore, the development of new types of phosphorus-reducing drug with fewer side effects faces severe challenges.

In order to improve the materials' therapeutic effects, metal organic frameworks (MOFs) as a new kind of porous complex,[16–22] which have been widely used in the fields of biosensing, catalysis, and photodynamic therapy due to their controllable synthesis, structural diversity and high specific surface area,[23–32] have raised our interest. Recently, our group designed nano-MOFs with Cu(II) as the active center to reduce glutathione levels and increase the concentration of ROS, thus strengthening the photodynamic efficiency and achieving a synergistic antitumor effect.[33] In this regard, we hypothesized that a Zr(IV)-based nano-MOF with an active center prone to specific phosphorus reactions would have the advantages of a large surface area and enhanced chemisorption abilities, as well as selective fluorescence sensing of phosphate to monitor

College of Chemistry, Chemical Engineering and Materials Science, Collaborative Innovation Center of Functionalized Probes for Chemical Imaging in Universities of Shandong, Key Laboratory of Molecular and Nano Probes, Ministry of Education, Institute of Biomedical Sciences, Shandong Normal University, Jinan 250014, P. R. China. E-mail: tangb@sdnu.edu.cn; zhangwei@sdnu.edu.cn

† Electronic supplementary information (ESI) available. See DOI: 10.1039/c8sc02638f

‡ These authors contributed equally to this work.

the process. Zr(IV) as the active center of the nano-MOF can specifically bind and absorb *in vivo* phosphate, thus directly decreasing the blood phosphorus levels and leading to a remission of hyperphosphatemia (Scheme 1). Notably, compared to commercially available phosphorus binders, the nano-MOF exhibits a greatly enhanced decrement in phosphorus levels. Finally, the hyperphosphatemia mice model with the MOF treatment further proved there was less *in vivo* toxicity and a better curing effect. This work provides strong evidence for MOFs as promising drugs for the treatment of hyperphosphatemia by directly adsorbing phosphorus in the blood, which will further optimize the clinical applications in the future.

Results and discussion

Characterization

Typically, porphyrin-inlaid Zr(IV)-based nano-MOF UiO-66 materials were prepared and characterized. The mechanical stability of the nano-MOFs was first investigated (Fig. 1a), where the PXRD patterns of the nano-MOF treated with PBS were consistent with those of the as-prepared MOFs, which proves decent crystalline stability in biological environments. By comparison with the FTIR absorptions of UiO-TCPP and UiO-66-NH_2, identical results were obtained (Fig. S1†) which suggests that porphyrin does not affect the crystal structure of the MOFs. The morphology and particle size of the MOFs were acquired through dynamic light scattering (DLS), SEM and TEM (Fig. 1b–d), which demonstrated the fine size control of the particles, which had a uniform distribution of 120 nm.

Fluorescence response

The fluorescence response of the MOFs to phosphate was studied *via* the two largest fluorescence emission peaks at 440 nm (2-aminoterephthalic acid) and 650 nm (porphyrin)

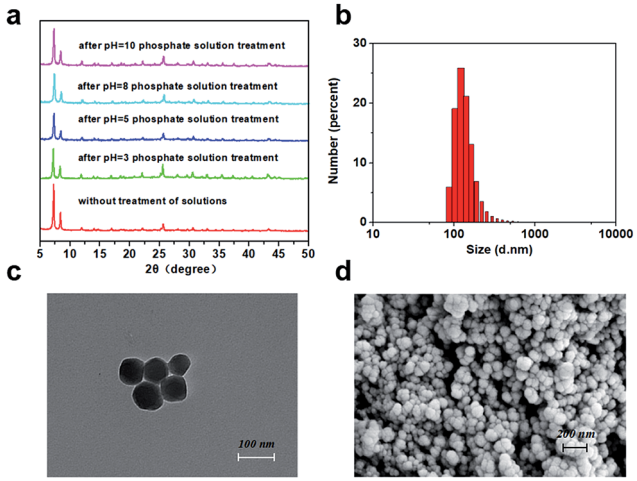

Fig. 1 (a) PXRD patterns for the as-synthesized samples of MOFs and the stability of the nano-MOFs in biological environments (red line, green line, blue line, light blue line and orange red line are the PXRD patterns for MOFs treated with PBS (2 mM) of pH 3, 5, 8 and 10 in 72 hours, respectively). (b) DLS image of the MOFs; (c) TEM image of the MOFs, scale bar = 100 nm; (d) SEM image of the MOFs, scale bar = 200 nm.

(Fig. S2†). By interacting with phosphate, the fluorescence intensities of MOFs were significantly enhanced due to the charge transfer interruption between the ligand molecule and the metal junction of the MOFs, and thus the ligand molecule's fluorescence was restored. To further explore the mechanism of the fluorescence intensity change caused by MOFs and phosphate, the fluorescence response of the MOFs to phosphate in the presence/absence of Zr(IV) ions was examined (Fig. S3†). Interestingly, no significant fluorescence change was observed when adding different concentrations of phosphate, which was attributed to Zr(IV) ions' preferential interactions with the phosphate. The Zr(IV) of the MOFs does not interact with phosphate, so there are no obvious changes in fluorescence

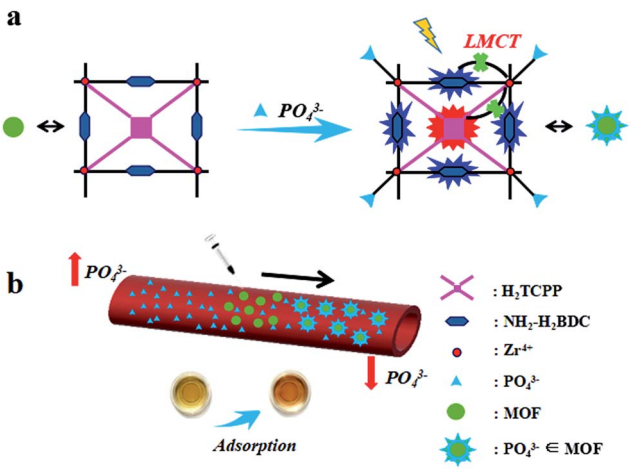

Scheme 1 Schematic diagram for the treatment of hyperphosphatemia based on Zr(IV)-MOFs. (a) Proposed mechanism of the fluorescence nanosensor for phosphate; (b) reduced levels of phosphate by MOFs for highly efficient treatment of hyperphosphatemia.

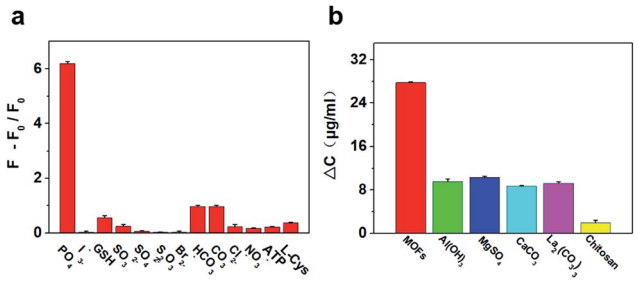

Fig. 2 (a) Fluorescence responses of MOFs with phosphate and other reactive small species. Relative fluorescence intensity ($F - F_0/F_0$) upon the addition of PO_4^{3-} (200 μM), I^- (100 nM), GSH (9.8 μM), SO_3^{2-} (100 nM), SO_4^{2-} (1.0 mM), $S_2O_3^{2-}$, Br^- (1.0 mM), HCO_3^- (1.0 mM), CO_3^{2-} (1.0 mM), Cl^- (1.0 mM), NO_3^- (1.0 mM), ATP (1.0 mM), and L-Cys (200 μM); (b) comparison of phosphate adsorption capacity by the MOF and other phosphorus binders measured using an ICP emission spectrometer. Experimental details: $C_{MOF} = 1$ mg mL^{-1}, other phosphorus binder concentrations: 1 mg mL^{-1}; fetal bovine serum (10-fold dilution, 10 mL).

Table 1 Baseline characteristics of the mouse model treated with the nano-MOF phosphorus binders *versus* the control[a]

Index	Cystatin C (mg L^{-1})	Creatinine (μmol L^{-1})	Phosphorus (mmol L^{-1})	Weight (g)	GFR
Normal	0.25 ± 0.00	50.83 ± 2.80	1.37 ± 0.08	43.56 ± 2.88	15.29
Model	0.50 ± 0.00	58.33 ± 2.80	2.15 ± 0.32	32.68 ± 3.23	9.79
Therapy	0.25 ± 0.00	47.50 ± 2.50	1.26 ± 0.45	35.56 ± 2.25	17.73

[a] GFR (estimated glomerular filtration rate) = 186 × (creatinine/88.14)$^{-1.154}$ × (weight/1000) was used to evaluate the renal function indicators of the mice.[34] The phosphorus levels was measured using an ICP emission spectrometer. The cystatin C and creatinine levels were evaluated using an automatic biochemical analyzer from Qilu Medical Research Institute.

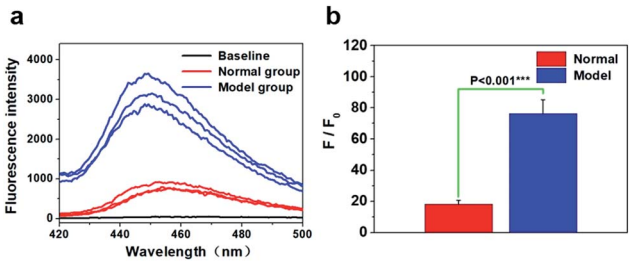

Fig. 3 (a) Fluorescence emission spectra of the MOFs upon the addition of a solution of the phosphate for the normal (red line) and model (blue line) groups; (b) data output of (a); *P* value less than 0.001, indicating significant differences between the two groups of data.

intensity, which further demonstrated the important role of Zr(IV) of MOFs for identification and fluorescence sensing of phosphate.

To thoroughly investigate the interactions between the MOFs and phosphate, the pH, concentration and response time were optimized (Fig. S4†). The fluorescence responses of the MOFs towards phosphate first increased greatly until 60 min, and then slowed down with the time extension, whilst a plateau was reached by 120 min. Under optimal conditions, the MOFs' phosphate absorption specificity was investigated using their fluorescence response (Fig. S5†). The phosphate was found to enhance the fluorescence intensities of MOFs (435 nm and 650 nm) with linear relationship ranges of 0.5–105 μM and 0.5–7 μM and correlation coefficients of 0.9987 and 0.9997, respectively. Based on the fluorescence response of the MOFs to phosphate, the material is used for fluorescence monitoring of the levels of phosphate in samples.

Selectivity

The MOFs' phosphate absorption selectivity was studied with the interference of common *in vivo* small molecular species. Fig. 2a shows that the fluorescence responses are significantly weaker for the ions even with higher concentrations than phosphate, representing a high selectivity of the MOFs towards phosphate. By further verification of the relationship between Zr(IV)-based MOFs and phosphate, UV-vis spectroscopy was carried out and an enhanced absorption at 420 nm was obtained after 1 h of incubation (Fig. S6†). This is most probably because phosphate, when binding to the MOFs' network architecture, influences the coordination between the metal center and the ligands, thus enhancing the absorption intensity

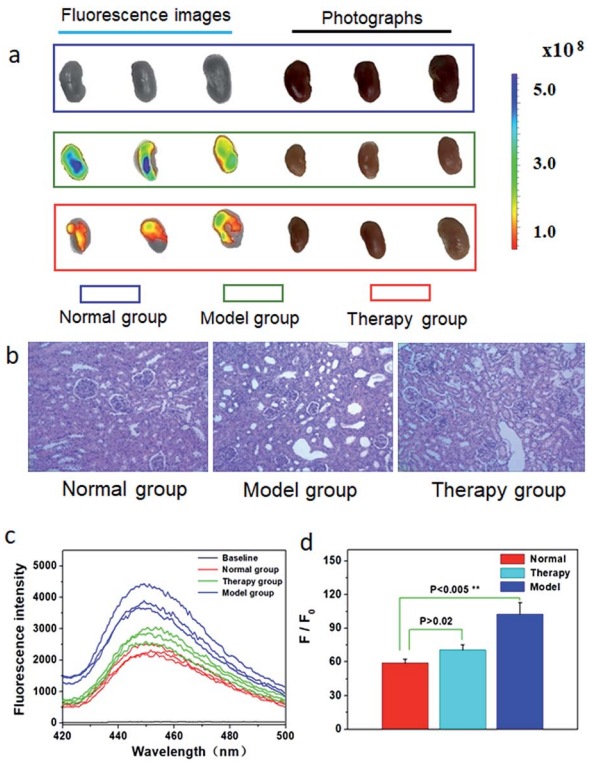

Fig. 4 (a) Fluorescence images of kidneys after treatment with nano-MOFs using an IVIS Lumina II *in vivo* imaging system with an open filter (670 ± 10 nm), and photographs of the kidneys, respectively; (b) kidney tissue slides of the MOF material which enters the bloodstream *via* stomach feeding; control: HEPES buffer was injected directly into the tumor section; (c) fluorescence emission spectra of the MOFs upon the addition of a solution of the phosphate for the normal and model groups after treatment with the nano-MOF; (d) data output of (c). *P* value more than 0.02, indicating no significant differences between the two groups of data.

of the porphyrin. UV-vis spectroscopy was performed to confirm the hypothesis by measuring the concentration of phosphate after incubating with MOFs (Fig. S7†), and 92.4 μg mg^{-1} was achieved, demonstrating a significant decrease from the phosphate solution, which means that the MOFs exhibit a significant adsorption capacity for phosphate.

Adsorption capacity

To improve the biocompatibility of the MOFs, the BSA protein was used to modify the MOFs' surface. The surface charge

changes of MOFs before and after modification with BSA were measured using the zeta potential. The potential increase from −13.7 mV to −3.5 mV (Fig. S8†) indicated that the BSA protein was successfully attached onto the surface of the MOFs (BSA-MOFs). Then, the hyperphosphatemia serum model was used to test if BSA-MOFs can reduce the levels of phosphate using UV-vis spectroscopy and an ICP emission spectrometer (Fig. S9†), and good efficacy was obtained in both characterizations. Subsequently, other commercially available phosphorus binders were compared with MOFs (Fig. 2b), but the MOFs exhibit obviously better adsorption capacities than all of the others. In addition, the MTT test showed the excellent biocompatibility of the MOFs *in vivo* (Fig. S10†). These results demonstrated that the MOFs directly adsorb phosphate, which remarkably reduces the phosphate levels.

Treatment of hyperphosphatemia in a mouse model

Then, a mouse model for chronic renal failure was established using adenine chemical induction. By measuring physiological indicators such as renal function, blood phosphorus levels, kidney tissue sections, body weight changes, and imaging of the mouse kidney tissue in normal and model mice, these results showed that all physiological indicators of the model mice were clearly distinguished from the normal mice, indicating successful establishment of a renal failure mouse model (Table 1 and Fig. 3 and 4). Therefore, the phosphate reducing efficacy by MOFs using the hyperphosphatemia mouse model was rationally tested.

Next, we tested the efficacy of the MOFs for lowering the phosphate levels using the hyperphosphatemia mouse model. After 10 days of treatment with MOFs in the stomachs of the mice, the physiological indicators were measured through different means. The serum phosphorus values and other indicators in the treated group are identical to those of the control group, indicating that the kidney metabolism of the treated group has mainly recovered to normal (Table 1). To verify whether the MOFs can relieve the symptoms of renal failure in mice, weight changes in mice in both groups were studied, and the treatment group has a slightly faster increase than the model group, which correlates with the hypothesis. As shown in Fig. 4a, the fluorescence images of kidney tissue (model group and therapy group) showed significant differences, suggesting the phosphorus levels in the kidneys have been significantly reduced. By comparing the kidney tissue slides (Fig. 4b), the renal tissue images of the treated group no longer exhibited dilation of the renal tubules compared with the model group, and more importantly, the treatment group had no pathological abnormalities of the renal tissues.

Finally, the levels of phosphate in the kidneys of the therapy group were measured based on the fluorescence of the nano-MOFs (Fig. 4c and d). It can be seen that there was no significant difference in fluorescence intensity, suggesting the phosphate levels between the treated group and the normal group had no significant difference. More importantly, the results measured using the fluorescence method were basically identical to those of other methods. These results confirmed that the phosphate levels in the treated group were remarkably reduced, and the physiological indicators of the mouse models were basically consistent with the normal mice, indicating that the hyperphosphatemia mouse model was effectively treated using the MOFs. In addition, the *in vivo* toxicity for the organs was tested to prove the biosafety of the MOF material as a phosphorus binding agent (Fig. S11†). Experiments on tissue slides (heart, liver, spleen and lung, respectively) were performed. Although the nano-MOFs enter the bloodstream *via* stomach feeding, the images showed the MOF material has less effect on other organs, which indicated that the nano-MOF has less *in vivo* toxicity.

Conclusions

In summary, as chronic kidney disease retains high levels of phosphorus in the blood, we have developed a nano-MOF with Zr(IV) as the active center to reduce the blood phosphorus levels and cure hyperphosphatemia by the direct adsorption of phosphorus. The highly porous MOFs offer significant numbers of Zr(IV) surface active centers for interactions, which dramatically reduce the phosphorus concentrations *in vivo*. By further comparisons with common *in vivo* small molecules and other phosphate binders, the MOFs possess high specificity and selectivity for reducing levels of phosphorus. Finally, the hyperphosphatemia mouse model with treatment using MOFs shows identical physiological parameters with the control group, representing promising biocompatibility for future applications. The present work provides not only a fluorescence nanosensor for monitoring blood phosphorus levels, but a new approach for effective hyperphosphatemia treatment in clinical therapies.

Conflicts of interest

There are no conflicts to declare.

Acknowledgements

This work was supported by the National Natural Science Foundation of China (21535004, 91753111 and 21390411), the Primary Research Plan in Shandong Province (2017GSF18196) and the Key Research and Development Program of Shandong Province (2018YFJH0502).

Notes and references

1 A. S. Levey and J. Coresh, *Lancet*, 2012, **379**, 165–180.
2 S. Mathew, K. S. Tustison, T. Sugatani, L. R. Chaudhary, L. Rifas and K. A. Hruska, *J. Am. Soc. Nephrol.*, 2008, **19**, 1092–1105.
3 N. Voormolen, M. Noordzij, D. C. Grootendorst, *et al.*, *Nephrol., Dial., Transplant.*, 2007, **22**, 2909–2916.
4 G. A. Block, P. S. Klassen, J. M. Lazarus, N. Ofsthun, E. G. Lowrie and G. M. Chertow, *J. Am. Soc. Nephrol.*, 2004, **15**, 2208–2218.

5 T. Isakova, O. M. Gutierrez, Y. Chang, A. Shah, H. Tamez, K. Smith, R. Thadhani and M. Wolf, *J. Am. Soc. Nephrol.*, 2009, **20**, 388–396.
6 K. J. Martin and E. A. Gonzalez, *Clin. J. Am. Soc. Nephrol.*, 2011, **6**, 440–446.
7 A. Levin, M. Tonelli, J. Bonventre, *et al.*, *Lancet*, 2017, **390**, 1888–1917.
8 A. Bellasi, M. Mandreoli, L. Baldrati, M. Corradini, P. D. Nicolo, G. Malmusi and A. Santoro, *Clin. J. Am. Soc. Nephrol.*, 2011, **6**, 883–891.
9 M. Yu, J. Zhou, B. Du, X. Ning, C. Authement, L. Gandee, P. Kapur, J. T. Hsieh and J. Zheng, *Angew. Chem., Int. Ed.*, 2016, **55**, 2787–2791.
10 J. Li, Y. Sun, C. Yang, Y. Zhu, H. Li and Z. Tong, *Med. Recapitulate*, 2017, **23**, 1557–1565.
11 J. Cashin and M. Battistella, *CANNT J.*, 2016, **26**, 17–21.
12 A. Covic, J. Passlick-Deetjen, M. Kroczak, B. Büschges-Seraphin, A. Ghenu, P. Ponce, B. Marzell and A. L. M. d. Francisco, *Nephrol., Dial., Transplant.*, 2013, **28**, 2383–2392.
13 S. A. Jamal, B. Vandermeer, P. Raggi, D. C. Mendelssohn, T. Chatterley, M. Dorgan, C. E. Lok, D. Fitchett and R. T. Tsuyuki, *Lancet*, 2013, **382**, 1268–1277.
14 G. Rombola, F. Londrino, V. Corbani, *et al.*, *J. Nephrol.*, 2012, **25**, 490–496.
15 C. Zhang, J. Wen, Z. Li and J. B. M. C. Fan, *J. Nephrol.*, 2013, **14**, 226.
16 M. O. Keeffe and O. M. Yaghi, *Chem. Rev.*, 2012, **112**, 675–702.
17 Y. Cui, B. Li, H. He, W. Zhou, B. L. Chen and G. D. Qian, *Acc. Chem. Res.*, 2016, **49**, 483–493.
18 C. He, D. Liu and W. B. Lin, *Chem. Rev.*, 2015, **115**, 11079–11108.
19 P. Ji, J. B. Solomon, Z. Lin, A. Johnson, R. F. Jordan and W. B. Lin, *J. Am. Chem. Soc.*, 2017, **139**, 11325–11328.
20 M. Yoon, R. Srirambalaji and K. Kim, *Chem. Rev.*, 2012, **112**, 1196–1231.
21 Y. Li, X. Zhao, H. Yin, G. Chen, S. Yang and Y. B. Dong, *Chem. Commun.*, 2016, **52**, 14113–14116.
22 J. Park, Q. Jiang, D. Feng, L. Mao and H. C. Zhou, *J. Am. Chem. Soc.*, 2016, **138**, 3518–3525.
23 M. Xu, S. Yuan, X. Y. Chen, Y. J. Chang, G. Day, Z. Y. Gu and H. C. Zhou, *J. Am. Chem. Soc.*, 2017, **139**, 8312–8319.
24 K. Y. A. Lin, S. Y. Chen and A. P. Jochems, *Mater. Chem. Phys.*, 2015, **160**, 168–176.
25 S. Wang, W. Morris, Y. Liu, C. M. McGuirk, Y. Zhou, J. T. Hupp, O. K. Farha and C. A. Mirkin, *Angew. Chem., Int. Ed.*, 2015, **54**, 14738–14742.
26 Y. Wang, Y. Xue, S. Li, X. Zhang, H. Fei, X. Wu, S. Sang, X. Li, M. Wei and W. Chen, *J. Polym. Res.*, 2017, **24**, 224.
27 W. P. Lustig, S. Mukherjee, N. D. Rudd, A. V. Desai, J. Li and S. K. Ghosh, *Chem. Soc. Rev.*, 2017, **46**, 3242–3285.
28 Y. Sun, L. Sun, D. Feng and H. C. Zhou, *Angew. Chem., Int. Ed.*, 2016, **55**, 6471–6475.
29 S. Wu, Y. Lin, J. Liu, W. Shi, G. Yang and P. Cheng, *Adv. Funct. Mater.*, 2018, **28**, 1707169.
30 J. Zhou, H. Li, H. Zhang, H. Li, W. Shi and P. Cheng, *Adv. Mater.*, 2015, **27**, 7072–7077.
31 H. Li, W. Shi, K. Zhao, Z. Niu, H. Li and P. Cheng, *Chem.–Eur. J.*, 2013, **19**, 3358–3365.
32 L. Wang, G. Fan, X. Xu, D. Chen, L. Wang, W. Shi and P. Cheng, *J. Mater. Chem. A*, 2017, **5**, 5541–5549.
33 W. Zhang, J. Lu, X. Gao, P. Li, W. Zhang, Y. Ma, H. Wang and B. Tang, *Angew. Chem., Int. Ed.*, 2018, **57**, 4891–4896.
34 A. S. Levey, L. A. Stevens, C. H. Schmid, Y. Zhang, A. F. Castro, H. I. Feldman, J. W. Kusek, P. Eggers, F. V. Lente, T. Greene and J. Coresh, *Ann. Intern. Med.*, 2009, **150**, 604–612.